



NJC

**Synthesis and molecular structure of arene ruthenium(II) benzhydrazone complexes: Impact of substitution at chelating ligand and arene moiety on antiproliferative activity**

|                               |   |
|-------------------------------|---|
| Journal:                      | <i>New Journal of Chemistry</i>   |
| Manuscript ID                 | NJ-ART-06-2016-001936.R2  |
| Article Type:                 | Paper   |
| Date Submitted by the Author: | 26-Sep-2016   |
| Complete List of Authors:     | Mohamed Kasim, Mohamed Subarkhan; Bharathidasan University, School of Chemistry<br>Rengan, Ramesh; Bharathidasan University, School of Chemistry;<br>Yu, Liu; Chinese Academy of Sciences, Institute of High Energy Physics |
|                               |   |

SCHOLARONE™  
Manuscripts

1                   **Synthesis and molecular structure of arene ruthenium(II)**  
2                   **benzhydrazone complexes: Impact of substitution at chelating**  
3                   **ligand and arene moiety on antiproliferative activity**

4 Mohamed Kasim Mohamed Subarkhan,<sup>†</sup> Rengan Ramesh,<sup>\*,†</sup> and Yu Liu<sup>‡</sup>

5 <sup>†</sup>Centre for Organometallic Chemistry, School of Chemistry, Bharathidasan University,  
6 Tiruchirappalli - 620 024, Tamil Nadu, India.

7 <sup>‡</sup>Institute of High Energy Physics, Chinese Academy of Sciences, Beijing 100 049, China.

8  
9 **Abstract**

10 Convenient method of synthesis of ruthenium(II) arene benzhydrazone complexes (**1-6**) of  
11 the general formula  $[(\eta^6\text{-arene})\text{Ru}(\text{L})\text{Cl}]$  (arene-benzene or *p*-cymene; L-monobasic bidentate  
12 substituted indole-3-carboxaldehyde benzhydrazone derivatives) has been described. The  
13 complexes have been fully characterized by elemental analysis, IR, UV-vis, NMR and ESI-  
14 MS spectral methods. The solid state molecular structures of representative complexes were  
15 determined by a single-crystal X-ray diffraction study and it indicates the presence of pseudo  
16 octahedral (piano stool) geometry. All the complexes were thoroughly screened for their  
17 cytotoxicity against human cervical cancer cells (HeLa), human breast cancer cell line  
18 (MDA-MB-231) and human liver carcinoma cells (Hep G2) under *in vitro* conditions.  
19 Interestingly, the cytotoxic activity of the complexes **3**, **4** and **6** are much more potent  
20 than cis-platin with low IC<sub>50</sub> values against all the cancer cell lines tested. Further, the  
21 mode of cell death in MDA-MB-231 cells was assessed by AO-EB staining, Hoechst 33258  
22 staining and flow cytometry technique along with comet assay. Further, the result of Western  
23 blot analysis suggests that complexes **3** and **6** were shown to accumulate preferentially in the  
24 mitochondria of MDA-MB-231 cells and induce apoptosis *via* mitochondrial pathway by up-  
25 regulating of p53 and Bax, and down-regulating Bcl-2.

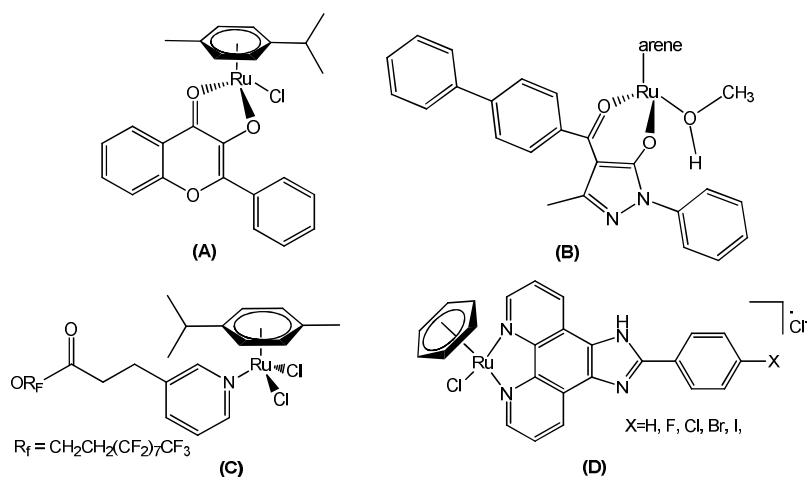
26  
27 **Introduction**

28 Over the past few decades, a large number of cisplatin analogs have been screened as  
29 potential antitumor agents, but of these only two, carboplatin and oxaliplatin, have entered  
30 world-wide clinical use.<sup>1</sup> Regardless of the achievements of current platinum drugs, they are  
31 efficient only for a limited range of cancers or some tumors can have acquired or intrinsic  
32 resistance, and they often cause severe side-effects.<sup>2,3</sup> Hence, there is a need for new

33 approaches that are purposefully designed to circumvent these drawbacks. In this regard,  
34 ruthenium compounds in +2 or +3 oxidation state are considered to be suitable candidates for  
35 anticancer drug design, since they exhibit a similar spectrum of kinetics for their ligand  
36 substitution reactions as platinum(II). A number of ruthenium compounds have been shown  
37 to display promising anticancer activity and two ruthenium(III) complexes have entered  
38 clinical trials, *trans*-[RuCl<sub>4</sub>(DMSO)(Im)]ImH (NAMI-A, where Im-imidazole),<sup>4</sup> and *trans*-  
39 [RuCl<sub>4</sub>(Ind)<sub>2</sub>]IndH (KP1019), where Ind-indazole.<sup>5</sup>

40 Several reports have been focused on the anticancer potential of half-sandwich Ru(II)  
41 arene complexes of the type, [(η<sup>6</sup>-arene)Ru(YZ)(X)], where Y and Z are bidentate chelating  
42 groups (NN, NO, OO, SO) or two monodentate ligands and X is a monodentate moiety, often  
43 a leaving group *e.g.* Cl have been extensively studied as anticancer agents.<sup>6</sup> These half-  
44 sandwich “piano-stool” complexes offer great scope for design, with the potential to vary  
45 each of the building blocks to allow modifications of thermodynamic and kinetic parameters.  
46 Indeed, it has been found that increasing the size of the coordinated arene increases their  
47 activity in the human ovarian cancer cell line. Changing the chelating ligand in these  
48 ruthenium arene complexes also appears to have an enormous effect on their kinetics and  
49 even changes their nucleobase selectivity.<sup>7</sup>

50 Synthesis and antiproliferative activity of Ru<sup>II</sup>(η<sup>6</sup>-arene) compounds carrying  
51 bioactive flavonol ligands have been reported by Hartinger *et al.* (A).<sup>8</sup> Wei Su *et al.* have  
52 described the DNA binding property and anticancer activity of ketone N4 substituted  
53 thiosemicarbazones and their ruthenium(II) arene complexes.<sup>9</sup> A series of ruthenium(II)  
54 arene complexes with the 4-(biphenyl-4-carbonyl)-3-methyl-1-phenyl-5-pyrazolonate ligand,  
55 and related 1,3,5-triaza-7-phosphaadamantane (PTA) derivatives, have been reported along  
56 with their anticancer activity with low IC<sub>50</sub> value (B).<sup>10</sup> Further, Dyson and his co-workers  
57 have reported the ruthenium(II)-arene complexes with a perfluoroalkyl-modified ligands  
58 displays remarkable *in vitro* cancer cell selectivity (C).<sup>11</sup> Recently, inhibitory activity of  
59 ruthenium(II) arene complexes of 2-phenylimidazole[4,5f] [1,10] phenanthroline against the  
60 migration and invasion of MDA-MB-231 breast cancer cells have been investigated (D)  
61 (Figure 1).<sup>12</sup>



62

63

**Figure 1.** Reported ruthenium(II) arene anticancer drugs.

64

65

66

67

68

69

70

71

72

73

In recent years, much attention was given to compounds with pharmacophore hydrazone moieties due to the identification of several hydrazone lead compounds showing antiproliferative activity<sup>13</sup> and antitumor activity.<sup>14</sup> It has been found from the literature that only a few reports are available on synthesis, characterisation and cytotoxicity of ruthenium(II) complexes containing hydrazone ligands.<sup>15</sup> Nevertheless, it should be pointed out that, as far as we know, the biological properties of arene ruthenium complexes bearing aroylhydrazones have not been studied so far. Therefore, in this study, we have combined ruthenium unit with a benzhydrazone ligand to generate a series of organometallic compounds with significant anticancer activity, taking advantage of the synthetic versatility of hydrazone derivatives and the promising biological activity.

74

75

76

77

78

79

80

81

82

83

84

85

We describe here, the synthesis and characterization of Ru(II) arene complexes containing bidentate indole-3-carboxaldehyde benzhydrazone ligands and chlorine. All the synthesized complexes have been characterized by elemental analysis, IR, UV-vis and NMR and ESI-MS spectroscopy techniques. The molecular structures of the complex **3** and **6** are confirmed through single crystal X-ray diffraction. The *in vitro* cytotoxicity of the complexes **1-6** against HeLa, MDA-MB-231, Hep G2 and NIH 3T3 were screened by MTT assay. The morphological changes were investigated using various apoptosis assays (AO-EB staining, Hoechst staining, flow cytometry technique and comet assay). Further, the apoptosis pathway was confirmed by change in the mitochondrial membrane potential and western blot analysis.

## 86 **Experimental Section**

### 87 **Methods and Instrumentation**

88 The microanalysis of carbon, hydrogen, nitrogen and sulphur were recorded by an  
89 analytical function testing Vario EL III CHNS elemental analyser at the sophisticated Test  
90 and Instrumentation Centre (STIC), Cochin University, Kochi. Melting points were recorded  
91 with a Boetius micro-heating table and are corrected. Thermal measurements (TGA/DTA)  
92 were carried out on Perkin Elmer Thermal Analyzer in nitrogen atmosphere with a heating  
93 rate of 10 °C min<sup>-1</sup>. FT-IR spectra were recorded in KBr pellets with JASCO 400 plus  
94 spectrometer. Electronic spectra in chloroform solution were recorded with a CARY 300 Bio  
95 UV- visible Varian spectrometer. <sup>1</sup>H NMR and <sup>13</sup>C-NMR were spectra were recorded on a  
96 Bruker 400 MHz instrument using tetramethylsilane (TMS) as an internal reference. A Micro  
97 mass Quattro II triple quadrupole mass spectrometer was employed for electrospray  
98 ionization mass spectrometry (ESI-MS). The theoretical calculations were performed using  
99 the IsoPro software.<sup>16</sup>

### 100 **Materials**

101 The starting materials [ $(\eta^6\text{-C}_6\text{H}_6)\text{RuCl}_2$ ]<sub>2</sub> and  $(\eta^6\text{-p-cymene})\text{RuCl}_2$ ]<sub>2</sub> were prepared  
102 according to literature methods.<sup>17</sup>

### 103 **Procedure for the preparation of indole-3-carboxaldehyde benzhydrazones ligands**

104 The ligands L1-L3 were prepared according to literature methods.<sup>18</sup> A mixture of 4-  
105 substituted benzhydrazide (R=H, Cl or OMe derivatives) (1 mmol) and indole-3-  
106 carboxaldehyde (1 mmol) in ethanol (10 mL) containing a drop of glacial acetic acid was  
107 refluxed for 30 min. The separated solid was filtered and dried in air. Ligands were further  
108 purified by recrystallisation from methanol. Yield: 67-92%.

109

### 110 **Procedure for the synthesis of ruthenium(II) arene benzhydrazone complexes**

111 A mixture containing starting [ $(\eta^6\text{-arene})\text{RuCl}_2$ ]<sub>2</sub> (arene-benzene or *p*-cymene) (0.05  
112 mmol), indole-3-carboxaldehyde benzhydrazone ligand (0.1 mmol) and triethylamine (0.3  
113 mL) in benzene (20 ml) was added and the resultant mixture was stirred at room temperature  
114 for 2 h. The orange brown precipitate was filtered, washed with hexane and dried in vacuo.  
115 The reaction progress was monitored through thin layer chromatography.

116 **[Ru( $\eta^6\text{-C}_6\text{H}_6$ )(Cl)(L1)] (1):** Brown solid. Yield = 0.160 g (68%); M.p.: 180°C (with  
117 decomposition); Calculated: C<sub>22</sub>H<sub>18</sub>ClN<sub>3</sub>ORu: C, 55.40; H, 3.80; N, 8.81 %. Found: C, 55.37;

118 H, 3.79; N, 8.82%. IR (KBr,  $\text{cm}^{-1}$ ): 1539  $\nu_{(\text{C}=\text{N}-\text{N}=\text{C})}$ , 1490  $\nu_{(\text{N}=\text{C}-\text{O})}$ , 1369  $\nu_{(\text{C}-\text{O})}$ . UV-Vis  
119 ( $\text{CH}_3\text{CN}$ ,  $\lambda_{\text{max}}/\text{nm}$ ;  $\epsilon/\text{dm}^3 \text{ mol}^{-1} \text{ cm}^{-1}$ ): 418 (1143), 273 (6371), 227 (14,757).  $^1\text{H}$  NMR (400  
120 MHz,  $\text{CDCl}_3$ ) ( $\delta$  ppm): 11.55 (br, 1H, indole N-H), 9.24 (s, 1H,  $\text{HC}=\text{N}$ ), 7.08–7.98 (m, 10H,  
121 aromatic), 5.72 (s, 6H, CH-benzene).  $^{13}\text{C}$  NMR (400 MHz,  $\text{CDCl}_3$ ) ( $\delta$  ppm) 164.15, 131.23,  
122 129.73, 129.52, 129.20, 128.50, 127.50, 127.18, 125.05, 123.45, 122.45, 117.10, 116.82,  
123 87.94 ppm. ESI-MS: displays a peak at  $m/z$  441.56 ( $\text{M} - \text{Cl}$ ) $^+$  (calcd  $m/z$  442.05).

124 **[Ru( $\eta^6$ -C<sub>6</sub>H<sub>6</sub>)(Cl)(L2)] (2)**: Brown solid. Yield = 0.0933 g (69%); M.p.: 172 $^\circ\text{C}$  (with  
125 decomposition); Calculated: C<sub>22</sub>H<sub>17</sub>Cl<sub>2</sub>N<sub>3</sub>ORu: C, 51.67; H, 3.35; N, 8.22 %. Found: C,  
126 51.68; H, 3.36; N, 8.20 %. IR (KBr,  $\text{cm}^{-1}$ ): 1531  $\nu_{(\text{C}=\text{N}-\text{N}=\text{C})}$ , 1487  $\nu_{(\text{N}=\text{C}-\text{O})}$ , 1378  $\nu_{(\text{C}-\text{O})}$ . UV-Vis  
127 ( $\text{CH}_3\text{CN}$ ,  $\lambda_{\text{max}}/\text{nm}$ ;  $\epsilon/\text{dm}^3 \text{ mol}^{-1} \text{ cm}^{-1}$ ): 419 (1044), 269 (4977), 233 (10,051).  $^1\text{H}$  NMR (400  
128 MHz,  $\text{CDCl}_3$ ) ( $\delta$  ppm): 11.45 (br, 1H, indole N-H), 9.35 (s, 1H,  $\text{HC}=\text{N}$ ), 6.78–7.92 (m, 9H,  
129 aromatic), 5.72 (s, 6H, CH-benzene).  $^{13}\text{C}$  NMR (400 MHz,  $\text{CDCl}_3$ ) ( $\delta$  ppm) 162.73, 159.67,  
130 130.61, 130.43, 129.30, 128.17, 114.54, 114.12, 88.57 ppm. ESI-MS: displays a peak at  $m/z$   
131 475.97 ( $\text{M} - \text{Cl}$ ) $^+$  (calcd  $m/z$  476.01).

132 **[Ru( $\eta^6$ -C<sub>6</sub>H<sub>6</sub>)(Cl)(L3)] (3)**: Orange brown solid. Yield = 0.268 g (92%); M.p.: 186 $^\circ\text{C}$  (with  
133 decomposition); Calculated C<sub>23</sub>H<sub>20</sub>ClN<sub>3</sub>O<sub>2</sub>Ru: C, 54.49; H, 3.98; N, 8.29 %. Found: C, 54.48;  
134 H, 4.00; N, 8.29 %. IR (KBr,  $\text{cm}^{-1}$ ): 1530  $\nu_{(\text{C}=\text{N}-\text{N}=\text{C})}$ , 1486  $\nu_{(\text{N}=\text{C}-\text{O})}$ , 1376  $\nu_{(\text{C}-\text{O})}$ . UV-Vis  
135 ( $\text{CH}_3\text{CN}$ ,  $\lambda_{\text{max}}/\text{nm}$ ;  $\epsilon/\text{dm}^3 \text{ mol}^{-1} \text{ cm}^{-1}$ ): 429 (1496), 268 (4904), 236 (10,242).  $^1\text{H}$  NMR (400  
136 MHz,  $\text{CDCl}_3$ ) ( $\delta$  ppm): 11.45 (br, 1H, indole N-H), 9.36 (s, 1H,  $\text{HC}=\text{N}$ ), 6.78–8.02 (m, 9H,  
137 aromatic), 5.72 (s, 6H, CH-benzene), 3.86 (s, 3H, OCH<sub>3</sub>).  $^{13}\text{C}$  NMR (400 MHz,  $\text{CDCl}_3$ ) ( $\delta$   
138 ppm) 163.98, 136.49, 131.52, 128.90, 128.42, 126.99, 124.97, 12.69, 117.55, 117.00, 114.27,  
139 114.27, 105.82, 88.94, 56.08 ppm. ESI-MS: displays a peak at  $m/z$  471.99 ( $\text{M} - \text{Cl}$ ) $^+$  (calcd  
140  $m/z$  472.06). Single crystals suitable for X-ray diffraction were obtained by recrystallisation  
141 in DCM and methanol solution.

142 **[Ru( $\eta^6$ -p-cymene)(Cl)(L1)] (4)**: Orange-brown solid. Yield = 0.240 g (80%); M.p.: 168 $^\circ\text{C}$   
143 (with decomposition); Calculated: C<sub>26</sub>H<sub>26</sub>ClN<sub>3</sub>ORu: C, 58.59; H, 4.92; N, 7.88 % Found: C,  
144 58.59; H, 4.97; N, 7.85%. IR (KBr,  $\text{cm}^{-1}$ ): 1528  $\nu_{(\text{C}=\text{N}-\text{N}=\text{C})}$ , 1486  $\nu_{(\text{N}=\text{C}-\text{O})}$ , 1371  $\nu_{(\text{C}-\text{O})}$ . UV-Vis  
145 ( $\text{CH}_3\text{CN}$ ,  $\lambda_{\text{max}}/\text{nm}$ ;  $\epsilon/\text{dm}^3 \text{ mol}^{-1} \text{ cm}^{-1}$ ): 431 (1044), 266 (4941), 228 (11,908).  $^1\text{H}$  NMR (400  
146 MHz,  $\text{CDCl}_3$ ) ( $\delta$  ppm): 11.86 (br, 1H, indole N-H), 9.29 (s, 1H,  $\text{HC}=\text{N}$ ), 6.95–8.33 (m, 10H,  
147 aromatic), 5.58 (d, 1H, p-cym-H), 5.43 (d, 1H, p-cym-H), 5.40 (d, 1H, p-cym-H), 5.32 (d,  
148 1H, p-cym-H), 2.85 (m, 1H, p-cym CH(CH<sub>3</sub>)<sub>2</sub>), 2.31 (s, 3H, p-cym CCH<sub>3</sub>), 1.28 (d, 3H, p-  
149 cym CH(CH<sub>3</sub>)<sub>2</sub>), 1.23 (d, 3H, p-cym CH(CH<sub>3</sub>)<sub>2</sub>).  $^{13}\text{C}$  NMR (400 MHz,  $\text{CDCl}_3$ ) ( $\delta$  ppm) 164.63,  
150 151.89, 147.82, 146.37, 131.61, 131.06, 129.65, 129.38, 128.68, 127.39, 125.25, 123.62,

151 123.13, 117.2, 116.06, 113.01, 32.25, 29.31, 27.07 ppm. ESI-MS: displays a peak at m/z  
152 497.62 (M - Cl)<sup>+</sup> (calcd m/z 498.12).

153 **[Ru( $\eta^6$ -p-cymene)(Cl)(L2)] (5):** brown solid. Yield = 0.269 g (82%); M.p.: 176<sup>o</sup>C (with  
154 decomposition); Calculated: C<sub>26</sub>H<sub>25</sub>Cl<sub>2</sub>N<sub>3</sub>ORu: C, 55.03; H, 4.44; N, 7.40 %. Found: C,  
155 55.06; H, 4.41; N, 7.42%. IR (KBr, cm<sup>-1</sup>): 1532  $\nu_{(C=N-N=C)}$ , 1481  $\nu_{(N=C-O)}$ , 1376  $\nu_{(C-O)}$ . UV-Vis  
156 (CH<sub>3</sub>CN,  $\lambda_{max}/nm$ ;  $\epsilon/dm^3 mol^{-1} cm^{-1}$ ): 410 (1237), 270 (6908), 232 (15,482). <sup>1</sup>H NMR (400  
157 MHz, CDCl<sub>3</sub>)  $\delta$  (ppm): 11.86 (br, 1H, indole N-H), 9.39 (s, 1H, HC=N), 6.98-7.62 (m, 9H,  
158 aromatic), 5.63 (d, 1H, p-cym-H), 5.50 (d, 1H, p-cym-H), 5.45 (d, 1H, p-cym-H), 5.38 (d,  
159 1H, p-cym-H), 3.10 (m, 1H, p-cym CH(CH<sub>3</sub>)<sub>2</sub>), 2.34 (s, 3H, p-cym CCH<sub>3</sub>), 1.40 (d, 3H, p-  
160 cym CH(CH<sub>3</sub>)<sub>2</sub>), 1.36 (d, 3H, p-cym CH(CH<sub>3</sub>)<sub>2</sub>). <sup>13</sup>C NMR (400 MHz, CDCl<sub>3</sub>) ( $\delta$  ppm) 164.15,  
161 131.23, 129.73, 129.52, 129.20, 128.50, 127.50, 127.18, 125.05, 123.45, 122.45, 117.10,  
162 116.82, 87.94 ppm. ESI-MS: displays a peak at m/z 531.21 (M - HCl)<sup>+</sup> (calcd m/z 532.08).

163 **[Ru( $\eta^6$ -p-cymene)(Cl)(L3)] (6):** Orange-brown solid. Yield = 0.180 g (78%); M.p.: 183<sup>o</sup>C  
164 (with decomposition); Calculated: C<sub>27</sub>H<sub>28</sub>ClN<sub>3</sub>O<sub>2</sub>Ru: C, 57.59; H, 5.01; N, 7.46 %. Found: C,  
165 57.59; H, 5.01; N, 7.47%. IR (KBr, cm<sup>-1</sup>): 1530  $\nu_{(C=N-N=C)}$ , 1485  $\nu_{(N=C-O)}$ , 1372  $\nu_{(C-O)}$ . UV-Vis  
166 (CH<sub>3</sub>CN,  $\lambda_{max}/nm$ ;  $\epsilon/dm^3 mol^{-1} cm^{-1}$ ): 427 (1576), 269 (7294), 229 (13,110). <sup>1</sup>H NMR (400  
167 MHz, CDCl<sub>3</sub>)  $\delta$  (ppm): 11.88 (br, 1H, indole N-H), 9.49 (s, 1H, HC=N), 6.74-8.58 (m, 9H,  
168 aromatic), 5.62 (d, 1H, p-cym-H), 5.47 (d, 1H, p-cym-H), 5.43 (d, 1H, p-cym-H), 5.36 (d,  
169 1H, p-cym-H), 3.81 (s, 3H, OCH<sub>3</sub>), 2.89 (m, 1H, p-cym CH(CH<sub>3</sub>)<sub>2</sub>), 2.34 (s, 3H, p-cym  
170 CCH<sub>3</sub>), 1.41 (d, 3H, p-cym CH(CH<sub>3</sub>)<sub>2</sub>), 1.37 (d, 3H, p-cym CH(CH<sub>3</sub>)<sub>2</sub>). <sup>13</sup>C NMR (400 MHz,  
171 CDCl<sub>3</sub>) ( $\delta$  ppm) 164.21, 147.73, 142.18, 132.99, 131.73, 131.66, 131.40, 130.01, 129.12,  
172 128.40, 127.65, 127.65, 127.12, 126.88, 124.94, 123.98, 117.44, 117.07, 32.16, 29.36, 27.14  
173 ppm. ESI-MS: displays a peak at m/z 527.86 (M - Cl)<sup>+</sup> (calcd m/z 528.13). Single crystals  
174 suitable for X-ray diffraction were obtained by recrystallisation in DCM and methanol  
175 solution.

176

### 177 X-ray crystallography

178 Single crystals of [Ru( $\eta^6$ -C<sub>6</sub>H<sub>6</sub>(Cl)(L3)] (3) and [Ru( $\eta^6$ -p-cymene)(Cl)(L3)] (6) were grown  
179 by slow evaporation of dichloromethane-methanol solution at room temperature. A single  
180 crystal of suitable size was covered with Paratone oil, mounted on the top of a glass fiber, and  
181 transferred to a Bruker AXS Kappa APEX II single crystal X-ray diffractometer using  
182 monochromated MoK $\alpha$  radiation ( $\lambda=0.71073$ ). Data were collected at 293K. The structure  
183 was solved with direct method using SIR-97 and was refined by full matrix least-squares

184 method on *F2* with SHELXL-97.<sup>19</sup> Non-hydrogen atoms were refined with anisotropy  
185 thermal parameters. All hydrogen atoms were geometrically fixed and collected to refine  
186 using a riding model. Frame integration and data reduction were performed using the Bruker  
187 SAINT Plus (Version 7.06a) software. The multi scan absorption corrections were applied to  
188 the data using SADABS software. Figure 1 was drawn with ORTEP<sup>20</sup> and the structural data  
189 deposited at The Cambridge Crystallographic Data Centre: CCDC **1499166** and **1498893**.

190

### 191 **Stability studies**

192 The stabilities of complexes **1–6** were checked by recording the UV-visible spectrum of them  
193 by dissolving in a minimum amount of 1% DMSO, and then diluted with PBS  
194 buffer. The hydrolysis profiles of these complexes were recorded by monitoring the  
195 electronic spectra for the resulting mixture over 24 h.

196

### 197 **Partition coefficients determination**

198 The hydrophobicity values of the complexes **1–6** were measured by the “Shake flask” method  
199 in octanol - water phase partitions as reported earlier. Complexes **1–6** (1 mg/mL) were  
200 dissolved in a mixture of water and *n*-octanol (2, 4, 6, 8, 10 µg/mL) followed by shaking for 1  
201 hour. The mixture was allowed to settle over a period of 30 minutes and the resulting two  
202 phases were collected separately without cross contamination of one solvent layer into  
203 another. The concentration of the complexes in each phase was determined by UV-Vis  
204 absorption spectroscopy at room temperature. The results are given as the mean values  
205 obtained from three independent experiments. The sample solution concentration was used to  
206 calculate  $\log P$ . Partition coefficients for **1–6** were calculated using the equation  $\log P =$   
207  $\log[(\mathbf{1-6})_{\text{oct}}/(\mathbf{1-6})_{\text{aq}}]$ .

208

### 209 **Cell culture and inhibition of cell growth.**

210 **Cell culture.** HeLa (human cervical cancer cell line), MDA-MB-231 (Triple negative  
211 breast carcinoma), Hep G2 (human liver carcinoma cell line) and NIH 3T3  
212 (noncancerous cell, mouse embryonic fibroblast) were obtained from the National Centre  
213 for Cell Science (NCCS), Pune. These cell lines were cultured as a monolayer in RPMI-1640  
214 medium (Biochrom AG, Berlin, Germany), supplemented with 10% fetal bovine serum  
215 (Sigma-Aldrich, St. Louis, MO, USA) and with 100 U mL<sup>-1</sup> penicillin and 100 µg mL<sup>-1</sup>  
216 streptomycin as antibiotics (Himedia, Mumbai, India), at 37 °C in a humidified atmosphere of  
217 5% CO<sub>2</sub> in a CO<sub>2</sub> incubator (Heraeus, Hanau, Germany).



### 218 **Inhibition of cell growth**

219 The IC<sub>50</sub> values, which are the concentrations of the tested compounds that inhibit  
220 50% of cell growth, were determined using a 3-(4,5-dimethyl thiazol-2-yl)-2,5-  
221 diphenyl tetrazolium bromide (MTT) assay. Cells were plated in their growth medium  
222 at a density of 5000 cells per well in 96 flat bottomed well plates. After 24 h plating,  
223 the benzhydrazone ligands and Ru(II) arene benzhydrazone complexes **1-6** were added  
224 at different concentrations (1-250 μM) for 24 h to study the dose dependent cytotoxic  
225 effect. To each well, 20 μL of 5 mg mL<sup>-1</sup> MTT in phosphate-buffer (PBS) was added.  
226 The plates were wrapped with aluminium foil and incubated for 4 h at 37 °C. The  
227 purple formazan product was dissolved by addition of 100 μL of 100% DMSO to each  
228 well. The quantity of formazan formed gave a measure of the number of viable cells.  
229 HeLa, MDA-MB-231 and Hep G2 were used for the MTT assay. The absorbance was  
230 monitored at 570 nm (measurement) and 630 nm (reference) using a 96 well plate  
231 reader (Bio-Rad, Hercules, CA, USA). Data were collected for four replicates each  
232 and used to calculate the respective means. The percentage of inhibition was  
233 calculated, from this data, using the formula: Percentage inhibition = 100 x {Mean OD  
234 of untreated cells (control) – Mean OD of treated cells} / {Mean OD of untreated cells  
235 (control)}. The IC<sub>50</sub> value was determined as the complex concentration that is  
236 required to reduce the absorbance to half that of the control.

237

### 238 **Acridine orange and ethidium bromide staining experiment**

239 The changes in chromatin organization in MDA-MB-231 cells after treatment with  
240 IC<sub>50</sub> concentration of the complexes **3** and **6** by using acridine orange (AO) and  
241 ethidium bromide (EB). Briefly, about 5 x 10<sup>5</sup> cells were allowed to adhere overnight  
242 on a coverslip placed in each well of a 12-well plate. The cells were allowed to recover  
243 for 1 h, washed thrice with DPBS, stained with an AO and EB mixture (1:1, 10 μM)  
244 for 15 min, and observed with epifluorescence microscope (Carl Zeiss, Germany).

245

### 246 **Hoechst 33258 staining method**

247 Hoechst 33258 staining was done using the method described earlier with slight  
248 modifications. 5 × 10<sup>5</sup> MDA-MB-231 cells were treated with IC<sub>50</sub> concentration of  
249 the complexes **3** and **6** for 24 h in a 6-well culture plate and were fixed with 4%  
250 paraformaldehyde followed by permeabilization with 0.1% Triton X-100. Cells were

251 then stained with  $50 \mu\text{g mL}^{-1}$  Hoechst 33258 for 30 min at room temperature. The cells  
252 undergoing apoptosis, represented by the morphological changes of apoptotic nuclei,  
253 were observed and imaged by epifluorescence microscope (Carl Zeiss, Germany).

254

#### 255 **Apoptosis evaluation - Flow cytometry**

256 The MDA-MB-231 cells were grown in a 6-well culture plate and exposed to  $\text{IC}_{50}$   
257 concentrations of complexes **3** and **6** for 24 h. The Annexin V-FITC kit uses annexin  
258 V conjugated with fluorescein isothiocyanate (FITC) to label phosphatidylserine sites  
259 on the membrane surface of apoptotic cells. Briefly the cells were trypsinised and  
260 washed with Annexin binding buffer and incubated with Annexin V-FITC and PI for  
261 30 minutes and immediately analysed using flow cytometer FACS Aria-II. The results  
262 were analysed using DIVA software and percentage positive cells were calculated.

263

#### 264 **Cellular DNA damage by the comet assay**

265 DNA damage was quantified by means of the comet assay as described. Assays were  
266 performed under red light at  $4 \text{ }^\circ\text{C}$ . Cells used for the comet assay were sampled from a  
267 monolayer during the growing phase, 24 h after seeding. MDA-MB-231 cells were  
268 treated with the complexes **3** and **6** at  $\text{IC}_{50}$  concentration, and cells were harvested by a  
269 trypsinization process at 24 h. A total of  $200 \mu\text{L}$  of 1% normal agarose in PBS at  $65 \text{ }^\circ\text{C}$   
270 was dropped gently onto a fully frosted microslide, covered immediately with a  
271 coverslip, and placed over a frozen ice pack for about 5 min. The coverslip was  
272 removed after the gel had set. The cell suspension from one fraction was mixed with  
273 1% low-melting agarose at  $37 \text{ }^\circ\text{C}$  in a 1:3 ratio. A total of  $100 \mu\text{L}$  of this mixture was  
274 applied quickly on top of the gel, coated over the microslide, and allowed to set as  
275 before. A third coating of  $100 \mu\text{L}$  of 1% low-melting agarose was placed on the gel  
276 containing the cell suspension and allowed to set. Similarly, slides were prepared (in  
277 duplicate) for each cell fraction. After solidification of the agarose, the coverslips were  
278 removed, and the slides were immersed in an ice-cold lysis solution (2.5 M NaCl, 100  
279 mM  $\text{Na}_2\text{EDTA}$ , 10 mM Tris, NaOH; pH 10, 0.1% Triton X-100) and placed in a  
280 refrigerator at  $4 \text{ }^\circ\text{C}$  for 16 h. All of the above operations were performed in low-  
281 lighting conditions in order to avoid additional DNA damage. Slides, after removal  
282 from the lysis solution, were placed horizontally in an electrophoresis tank. The  
283 reservoirs were filled with an electrophoresis buffer (300 mM NaOH and 1 mM

284 Na<sub>2</sub>EDTA, pH > 13) until the slides were just immersed in it. The slides were allowed  
285 to stand in the buffer for about 20 min (to allow DNA unwinding), after which  
286 electrophoresis was carried out at 0.8 v cm<sup>-1</sup> for 15 min. After electrophoresis, the  
287 slides were removed, washed thrice in a neutralization buffer (0.4 M Tris, pH 7.5), and  
288 gently dabbed to dry. Nuclear DNA was stained with 20 μL of EB (50 μg mL<sup>-1</sup>).  
289 Photographs were taken using an epifluorescence microscope (Carl Zeiss).

290

### 291 **Mitochondrial membrane potential Assay**

292 Mitochondrial membrane potential,  $\Delta\psi_m$  is an important parameter of mitochondrial  
293 function used as an indicator of cell health. MDA-MB-231 cells treated overnight with  
294 IC<sub>50</sub> concentration of the complexes **3** and **6** in 6-well plates were incubated for 1 h  
295 with 2 μg mL<sup>-1</sup> of JC-1 in the culture medium. The adherent cell layer was then  
296 washed three times with PBS and dislodged with 250 μL of trypsin-EDTA. Cells were  
297 collected in PBS/2% bovine serum albumin (BSA), washed twice by centrifugation,  
298 resuspended in 0.3 mL of PBS/2% BSA, mixed gently, and examined in the  
299 fluorescent microscope (Carl Zeiss, Jena, Germany).

300

### 301 **Western blot analysis**

302 For Western blotting, MDA-MB-231 cells were treated with the complexes **3** and **6** at  
303 IC<sub>50</sub> concentration for 24 h, and appropriate amounts of cell lysates (25 μg protein)  
304 were resolved over 10% Tris-glycine polyacrylamide gel, and then transferred onto  
305 the PVDF membrane. The blots were blocked using 5% non-fat dry milk and probed  
306 using p53, Bcl-2 and Bax primary monoclonal antibodies in blocking buffer overnight  
307 at 4 °C. The membrane was then incubated with appropriate secondary antibody-  
308 horseradish peroxidase conjugate (Amersham Life Sciences Inc., IL, USA), followed  
309 by detection using chemiluminescence ECL kit (Amersham Life Sciences Inc., IL,  
310 USA). To ensure equal loading of protein, the membrane was stripped and reprobbed  
311 with anti-β-actin antibody (Sigma Aldrich, USA).

312

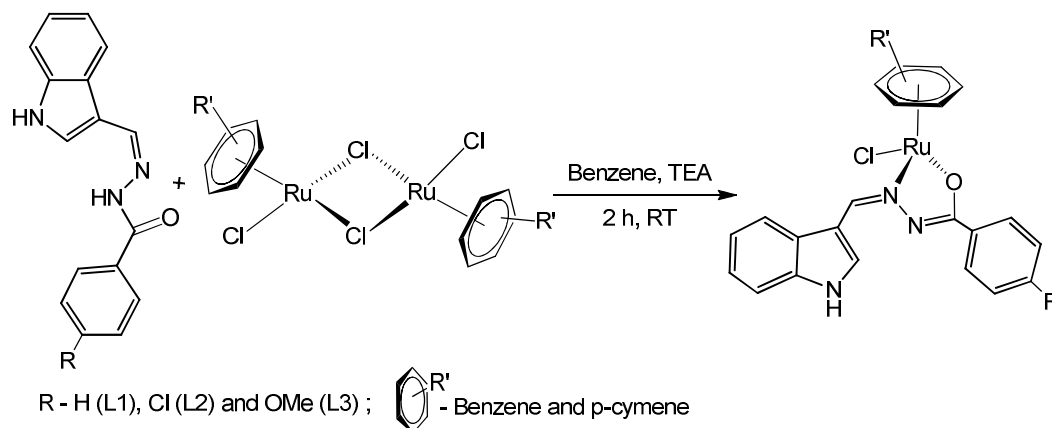
## 313 **Results and Discussion**

### 314 **Synthesis of ruthenium(II) arene benzhydrazone complexes**

315 The hydrazone ligand derivatives were conveniently prepared in an excellent yield by  
316 the condensation of indole-3-carboxaldehyde with 4-substituted benzhydrazides (H, Cl and

317 OMe derivatives) in an equimolar ratio.<sup>17</sup> These ligands were allowed to react with the  
 318 ruthenium(II) arene precursor  $[(\eta^6\text{-arene})\text{RuCl}_2]_2$  (arene-benzene or *p*-cymene) in a 2:1 molar  
 319 ratio in the presence of triethylamine as the base and the new complexes of the general  
 320 formula,  $[(\eta^6\text{-arene})\text{Ru}(\text{L})\text{Cl}]$  (arene-benzene or *p*-cymene; L-substituted indole-3-  
 321 carboxaldehyde benzhydrazone derivatives) (**Scheme 1**) were obtained in high yields. The  
 322 addition of triethylamine to the reaction mixture was used to remove a proton from the imidol  
 323 oxygen and to facilitate the coordination of the imidolate oxygen to the ruthenium(II) ion. All  
 324 complexes are air-stable and are highly soluble in most organic solvents. The analytical data  
 325 of all the ruthenium(II) arene benzhydrazone complexes are in good agreement with the  
 326 molecular formula proposed.

327



328

329 **Scheme 1.** Synthesis of ruthenium(II) arene indole-3-carboxaldehyde benzhydrazone  
 330 complexes

### 331 Characterization of the complexes

332 The IR spectra of the free ligands displayed a medium to strong band in the region of  
 333 3180- 3196  $\text{cm}^{-1}$  which is characteristic of the N-H functional group. The free ligands also  
 334 displayed  $\nu_{\text{C=N}}$  and  $\nu_{\text{C=O}}$  absorptions in the region of 1548-1576  $\text{cm}^{-1}$  and 1610-1653  $\text{cm}^{-1}$   
 335 respectively, which indicate that the ligands exist in the amide form in the solid state. Bands  
 336 that are due to  $\nu_{\text{N-H}}$  and  $\nu_{\text{C=O}}$  stretching vibrations were not observed with the complexes,  
 337 which indicates that the ligands underwent tautomerization and subsequent coordination of  
 338 the imidolate enolate form during complexation. Coordination of the ligand to the  
 339 ruthenium(II) ion through an azomethine nitrogen is expected to reduce the electron density  
 340 in the azomethine link and thus lower the absorption frequency upon complexation 1528-  
 341 1539  $\text{cm}^{-1}$  which indicates the coordination of azomethine nitrogen to the ruthenium(II) ion.  
 342 The band in the region of 1369-1378  $\text{cm}^{-1}$  is due to the imidolate oxygen, which is

343 coordinated to the metal. The IR spectra of all the complexes therefore confirm the mode of  
344 coordination of the benzhydrazone ligand to the ruthenium(II) ion *via* the azomethine  
345 nitrogen and imidolate oxygen.<sup>21</sup>

346 The absorption spectra of the ruthenium(II) arene benzhydrazone complexes in  
347 chloroform exhibited very intense band around 266-273 nm and 227-236 nm are assigned to  
348 ligand-centered (LC)  $\pi$ - $\pi^*$  and  $n$ - $\pi^*$  transitions respectively. The lowest energy absorption  
349 bands in the electronic spectra of the complexes in the visible region 410-431 nm are ascribed  
350 to MLCT (metal to ligand charge transfer) transitions. Based on the pattern of the electronic  
351 spectra of all the complexes an octahedral environment around the ruthenium(II) ion has been  
352 proposed similar to that of the other octahedral ruthenium(II) arene complexes.<sup>22</sup>

353 The <sup>1</sup>H NMR spectra of all the complexes were recorded in CDCl<sub>3</sub> to confirm the  
354 bonding of the benzoylhydrazone ligand to the ruthenium(II) ion. Multiplets observed in the  
355 region  $\delta$  6.74-8.61 ppm in the complexes have been assigned to the aromatic protons of  
356 benzhydrazone ligands. The signal due to the azomethine proton appears in the region  $\delta$  9.24-  
357 9.49 ppm. The position of the azomethine signal in the complexes is slightly downfield in  
358 comparison with that of the free ligand, suggesting deshielding of the azomethine proton due  
359 to its coordination to ruthenium. The singlet due to the -NH proton of the free ligand in the  
360 region  $\delta$  11.22-11.60 ppm is absent in the complex, further supporting enolisation and  
361 coordination of the imidolate oxygen to the Ru(II) ion. Therefore, the <sup>1</sup>H NMR spectra of the  
362 complexes confirm the bidentate coordination mode of the benzhydrazone ligands to  
363 ruthenium(II) ion. In all the complexes, the indole N-H protons are observed as singlets in  
364 between  $\delta$  11.41-11.88 ppm. The cymene protons are appeared in the region of  $\delta$  5.32-5.62  
365 ppm.<sup>23</sup> In addition, the two isopropyl methyl protons of the p-cymene appeared as two  
366 doublet in the region of  $\delta$  1.23-1.41 ppm and the methine protons comes in the region of  $\delta$   
367 2.31-3.10 ppm as septet. Further, the methyl group of the p-cymene comes as singlet around  
368 the region of  $\delta$  2.31-2.34 ppm. Additionally methoxy protons are observed as singlet for  
369 complexes **3** and **6** at  $\delta$  3.81-3.86 ppm. On the other hand, benzene arene protons displayed  
370 an upfield shift relative to complex **4-6** in the region  $\delta$  5.72-5.73 ppm. (Figure S1, Supporting  
371 Information). The <sup>13</sup>C NMR of the Ru(II) arene complexes showed resonance in the expected  
372 regions (Figure S2, Supplementary material) and the complex revealed a downfield shift of  
373 the azomethine carbon relative to the free ligands indicating coordination of the azomethine  
374 nitrogen to the metal centre.

375

### 376 **Stability of Complexes (Time-Dependent Spectra).**

377 Stability in solution is an important requirement for drug candidates. The stability of  
378 the most cytotoxic complexes **1-6**, was studied by UV–Vis spectroscopy in a solution of 1%  
379 DMSO in PBS. All the ruthenium(II) arene benzhydrazone complexes showed characteristic  
380 peaks in the region of 200-800 nm and did not exhibit any significant changes during a 24-  
381 hour period. The absence of significant changes in the peak absorptions and spectral  
382 characteristics for tested complexes over time may suggest that no structural alternations  
383 occurred in buffer solution. The data for all studied complexes is presented in Figure S5,  
384 (Supporting Information). Further, the composition of the complexes has been studied by  
385 ESI-MS spectral studies. Mass spectrometric measurements carried out under positive ion  
386 ESI mode using acetonitrile as the solvent. In their positive ESI mass spectra **1-6** showed  
387 major peaks due to cationic fragment  $[(\eta^6\text{-arene})\text{Ru}(\text{L})\text{Cl}]^+$  generated by loss of the  $\text{Cl}^-$ . The  
388 ESI spectra of complexes 1-6 display at  $m/z$  found (calcd): [441.56 (442.05) (**1**, M -  $\text{Cl}^+$ )],  
389 [475.97 (476.01) (**2**, M -  $\text{Cl}^+$ )], [471.99 (472.06) (**3**, M -  $\text{Cl}^+$ )], [497.62 (498.12) (**4**, M -  $\text{Cl}^+$ )],  
390 [531.21 (532.08) (**5**, M -  $\text{HCl}^+$ )] and [527.86 (528.13) (**6**, M -  $\text{Cl}^+$ )] respectively confirm the  
391 presence of monomeric entity in solution phase. The mass spectrometry results are in good  
392 agreement with the proposed molecular formulae of the complexes and suggest that chloro  
393 ( $\text{Cl}^-$ ) group is labile and possibly replaced by targeted biomolecules. The experimentally  
394 observed and theoretically calculated isotopic distributions were in excellent agreement with  
395 each other as illustrated in and are shown in Figure S3 and S4, (Supporting Information).  
396 Further, the thermal stability of the synthesized ruthenium(II) arene complexes **3** and **6** was  
397 determined by thermogravimetric analysis (TGA) and differential thermal analysis (DTA) as  
398 shown in S6 (Supporting Information). The synthesized complex is stable up to 180 °C. The  
399 results are in good agreement with the formulae suggested from the analytical data.

400

### 401 **X-ray crystallographic studies**

402 Attempts were made to grow single crystals for all the complexes to confirm the  
403 coordination mode of the ligand to metal and geometry of the complex. However we could  
404 not obtain single crystals for complexes  $[\text{Ru}(\eta^6\text{-p-cymene})(\text{Cl})(\text{L3})]$  (**3**) and  $[\text{Ru}(\eta^6\text{-}$   
405  $\text{C}_6\text{H}_6)(\text{Cl})(\text{L3})]$  (**6**). Crystals of **3** and **6** grew from slow diffusion of dichloromethane into  
406 methanol solutions and crystallized in the monoclinic system with P2(1)/n space group. The  
407 selected bond lengths and bond angles are given in Table 1 whereas crystallographic data and  
408 structural refinement parameters are gathered in Table S1 (Supporting Information). The

409 ORTEP views of the molecules with the atom numbering are shown in Figures 2 and 3. The  
 410 molecular structure of the complex **3** shows clearly that the benzhydrazone ligand coordinates  
 411 in a bidentate manner to ruthenium ion *via* the azomethine nitrogen and imidolate oxygen in  
 412 addition to one chlorine and one arene group. The complex adopts the commonly observed  
 413 piano-stool geometry as reported in many half-sandwich arene ruthenium(II) complexes.<sup>24</sup> In  
 414 this case, the arene ring forms the seat of the piano-stool, while the bidentate benzhydrazone  
 415 N, O and Cl ligands form the three legs of the stool. Therefore, ruthenium(II) ion is sitting in  
 416 a NOCl ( $\eta^6$ -arene) coordination environment. The benzhydrazone ligand bind to the metal  
 417 centre at N and O forming the five membered chelate ring with bite angle 76.18(12) $^\circ$  O(1)-  
 418 Ru(1)-N(2) and 84.26(11) $^\circ$  N(2)-Ru(1)-Cl(1). The bond lengths of Ru(1)-N(2) and Ru(1)-  
 419 O(1) are 2.069(3) Å and 2.069(3) Å respectively. The Ru-Cl bond length is found to be  
 420 2.4233(13) Å and the bond length is in agreement with other structurally characterized *p*-  
 421 cymene ruthenium complexes.<sup>25</sup> The ruthenium atom is  $\pi$  bonded to the arene ring with an  
 422 average Ru-C distance of 2.156(7) Å, whereas average C-C bond length in the arene ring is  
 423 1.425(8) Å with alternating short and long bonds. It was observed that the complex **6** also  
 424 adopt similar geometrical environment as in the complex **3** with slight variation in the bond  
 425 angles and bond distances. The crystal structures of **3** and **6** revealed the presence of  
 426 extensive intermolecular hydrogen bonding interactions shown in (Figure S7, Supporting  
 427 Information).

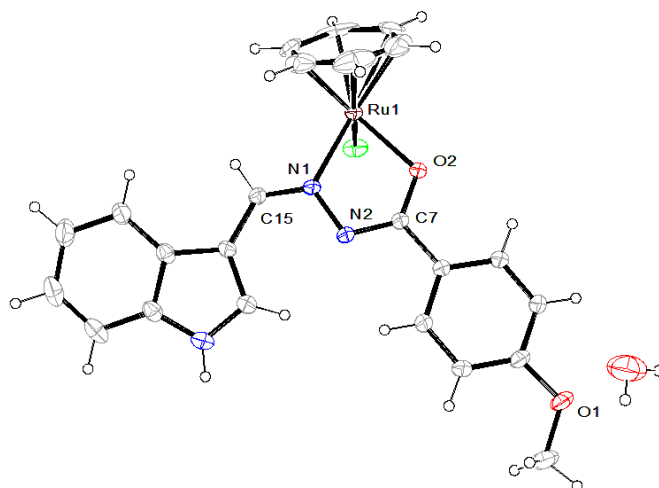
428

429 **Table 1.** Selected Bond Lengths (Å) and Angles ( $^\circ$ ) in **3**.H<sub>2</sub>O and **6**.

| distances/angles | <b>3</b> .H <sub>2</sub> O | <b>6</b>   |
|------------------|----------------------------|------------|
| Ru1-N2           | 2.069(3)                   | 2.077(4)   |
| Ru1-O1           | 2.069(3)                   | 2.065(4)   |
| Ru1-Cl1          | 2.4233(13)                 | 2.4060(16) |
| Ru1-C22          | 2.156(7)                   | 2.153(5)   |
| N1-N2            | 1.391(5)                   | 1.389(6)   |
| N2-C7            | 1.326(6)                   | 1.326(6)   |
| O2-C9            | 1.289(5)                   | 1.289(6)   |
| O1-Ru1-N2        | 76.18(12)                  | 75.71(16)  |
| N2-Ru1-Cl1       | 84.26(11)                  | 83.85(13)  |
| N2-N1-Ru1        | 116.0(2)                   | 115.7(3)   |
| C7-O1-Ru1        | 112.8(2)                   | 112.8(3)   |
| C7-N2-N1         | 110.5(3)                   | 110.6(4)   |
| C19-Ru1-Cl1      | 106.2 (3)                  | 104.81(16) |
| O1-Ru1-Cl1       | 84.46(10)                  | 86.90(12)  |

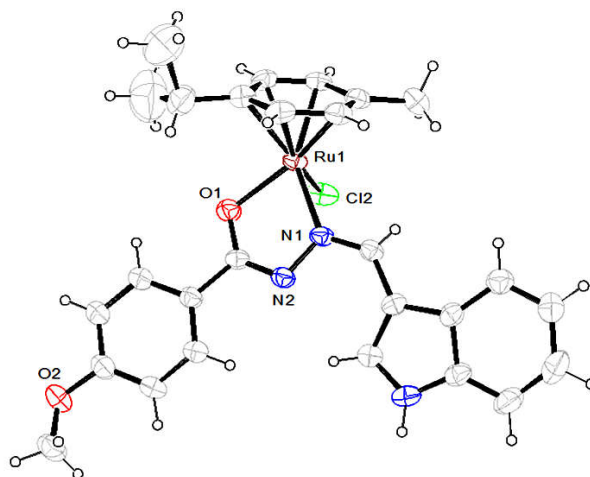
430

431



432

433 **Figure 2.** ORTEP drawing of complex **3**.H<sub>2</sub>O at 30% probability level.



434

435 **Figure 3.** ORTEP drawing of complex **6** at 30% probability level.

436

### 437 Partition coefficients determination

438 Lipophilicity is an important factor for the cellular accumulation and oral bioavailability of  
 439 drugs. It is often expressed as the n-octanol/water partition coefficient ( $\log P$ ), which is also a  
 440 central parameter in many in silico medicinal chemistry approaches, such as the  
 441 determination of the drug likeliness of a new drug. This was investigated by the partition  
 442 coefficient,  $P$  a parameter, which indicates the hydrophobic character of molecules and their  
 443 ability to cross lipid bilayers.<sup>26</sup> The calculated  $\log P$  values for complexes **1-6** are 2.59, 2.72,  
 444 2.48, 2.23, 2.35 and 1.99 respectively. It has been observed that complex **6** with a p-cymene  
 445 group shows higher potency than the rest of the complexes (Table 2).

446



**447 *In Vitro* antiproliferative activity**

448 All the ruthenium complexes and the free benzhydrazone ligands evaluated for their  
449 cytotoxic activity against HeLa, MDA-MB-231 and Hep-G2 along with NIH 3T3 cell  
450 lines by using colorimetric assay (MTT assay) that measures mitochondrial dehydrogenase  
451 activity as an indication of cell viability. The effects of the ruthenium(II) arene complexes to  
452 arrest the proliferation of cancer cells were evaluated after an exposure of 24 h. It is to be  
453 noted that the ligands did not show any inhibition of the cell growth even up to 100  $\mu\text{M}$  and  
454 clearly indicates chelation of the ligand with metal ion is responsible for the observed  
455 cytotoxicity properties of the complexes. The results of MTT assays revealed that complexes  
456 showed notable activity against the cell lines HeLa, MDA-MB-231 and Hep-G2 with  
457 respect to  $\text{IC}_{50}$  values (Table 2). From the  $\text{IC}_{50}$  values obtained it was inferred that complexes  
458 **3**, **4** and **6** are highly active against all the cell lines with very low  $\text{IC}_{50}$  values than that of the  
459 well-known anticancer drug cisplatin. In addition, the *in vitro* cytotoxic activity studies of the  
460 complexes against the mouse embryonic fibroblast cell line NIH 3T3 (normal cells) was  
461 undertaken and the  $\text{IC}_{50}$  values are above 215  $\mu\text{M}$ , which confirmed that the complexes are  
462 very specific on cancer cells.

463 These ruthenium(II) arene benzhydrazone complexes **1-6** possess significant  
464 cytotoxicity over the ligands may be due to the presence of extended  $\pi$  conjugation resulting  
465 from the chelation of Ru(II) ion with the ligand. Further, the observed higher activity of the  
466 complexes **4** and **6** is correlated to the nature of the chelating benzoylhydrazone ligand and  
467 arene moiety. Further, the observed higher activity of the complexes **3** and **6** is correlated to  
468 the nature of the chelating benzhydrazone ligand and arene moiety. In the complexes **3** and **6**,  
469 the presence of electron donating methoxy substituent at phenyl ring of the ligand increases  
470 the lipophilic character of the metal complex, which favours its permeation through the lipid  
471 layer of a cell membrane.

472 On the other hand, the arene groups also play an important role in the antitumor  
473 activity of these ruthenium complexes. It has been observed that complex **6** with a p-cymene  
474 group show higher potency than those with a benzene group in complex **3**, which may be  
475 attributed to the stronger hydrophobic interactions between the Ru (II)-cymene complex and  
476 the biomolecular targets as evidenced by partition coefficient value.<sup>27</sup> Complex **6** shows high  
477 cytotoxic activity with very low  $\text{IC}_{50}$  values of  $11.4 \pm 0.7$ ,  $4.1 \pm 0.4$  and  $9.1 \pm 0.3$   $\mu\text{M}$  toward  
478 HeLa, MDA-MB-231 and Hep-G2. Further, the  $\text{IC}_{50}$  values are much better than those  
479 previously reported for other Ru(II) arene arylazo, 2-thiosalicylic acid, phenanthroimidazole

480 or polypyridyl complexes.<sup>28,10</sup> The excellent results suggest to investigate the underlying  
 481 mechanism accounting for the antiproliferative action of these ruthenium arene  
 482 benzhydrazone complexes.

483

484 **Table 2.** Cytotoxicity (IC<sub>50</sub>, μM) of ligand and complexes **1-6**. (n.e.: no effect) and calculated  
 485 partition coefficients (log *P*).

| Complex          | IC <sub>50</sub> values (μM) |            |            |             | log <i>P</i> |
|------------------|------------------------------|------------|------------|-------------|--------------|
|                  | HeLa                         | MDA-MB-231 | Hep G2     | NIH3T3      |              |
| Complex <b>1</b> | 20.8 ± 0.2                   | 18.2 ± 0.8 | 14.2 ± 0.3 | 223.9 ± 0.7 | 2.59 ± 0.4   |
| Complex <b>2</b> | 25.9 ± 0.8                   | 19.9 ± 0.1 | 16.8 ± 0.5 | 215.3 ± 0.6 | 2.72 ± 0.3   |
| Complex <b>3</b> | 19.4 ± 0.3                   | 15.3 ± 0.3 | 13.4 ± 0.4 | 235.4 ± 0.3 | 2.48 ± 0.3   |
| Complex <b>4</b> | 13.6 ± 0.4                   | 11.2 ± 0.3 | 11.6 ± 0.4 | 230.4 ± 0.5 | 2.23 ± 0.2   |
| Complex <b>5</b> | 17.9 ± 0.3                   | 12.8 ± 0.2 | 12.8 ± 0.1 | 224.3 ± 0.8 | 2.35 ± 0.3   |
| Complex <b>6</b> | 11.4 ± 0.7                   | 4.1 ± 0.4  | 9.1 ± 0.3  | 241.3 ± 0.4 | 1.99 ± 0.2   |
| L1               | n.e.                         | n.e.       | n.e.       | n.e.        |              |
| L2               | n.e.                         | n.e.       | n.e.       | n.e.        |              |
| L3               | n.e.                         | 91.7 ± 0.5 | 94.7 ± 0.9 | n.e.        |              |
| Cisplatin        | 19.2 ± 1.1                   | 12.9 ± 0.6 | 20.1 ± 1.2 | 212.3 ± 0.6 |              |

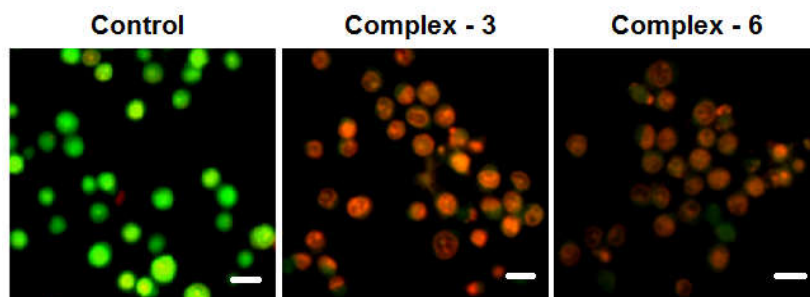
486 The ligands L1-L3 were added at different concentrations (1-250 μM) for 24 h.

487

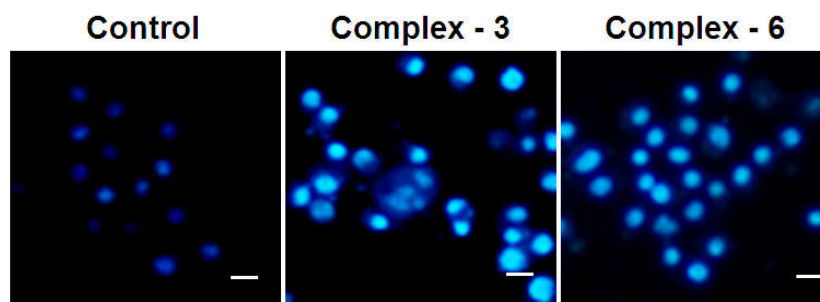
#### 488 **AO-EB and Hoechst staining assays**

489 Acridine orange and ethidium bromide (AO and EB) dual staining followed by  
 490 fluorescence microscopy revealed apoptosis from the perspective of fluorescence  
 491 emission. Apoptosis is characterized by cell shrinkage, blebbing of the plasma  
 492 membrane and chromatin condensation. To identify apoptosis, at a basic level, we  
 493 adopted AO-EB staining to visualize and quantify the number of viable and apoptic  
 494 cells. According to the difference in membrane integrity between necrotic and  
 495 apoptosis, AO can pass through cell membrane, but EB cannot. After the treatment of  
 496 MDA-MB-231 cells with complexes **3** and **6** for 24 h at IC<sub>50</sub> concentration, the  
 497 apoptotic effect is shown in Figure 4. The cells incubated with the complexes **3** and **6**  
 498 for 2 h and irradiated with visible light showed significant reddish-orange emission  
 499 characteristic of the apoptotic cells. In the control, the cells of MDA-MB-231 were  
 500 stained bright green in spots. Additionally complexes **3** and **6** treated MDA-MB-231

501 cells were stained with Hoechst 33258, apoptotic features such as nuclear shrinkage  
502 and chromatin condensation were also observed (Figure 5). Hence the results of AO-  
503 EB and Hoechst staining assays suggest that complexes **3** and **6** induce apoptosis in  
504 MDA-MB-231 cells.<sup>28-29</sup>



505  
506 **Figure 4.** Morphological assessment of AO and EB of MDA-MB-231 cells treated with  
507 complexes **3** and **6** ( $IC_{50}$  concentration) for 24 h. The scale bar 20  $\mu$ m.

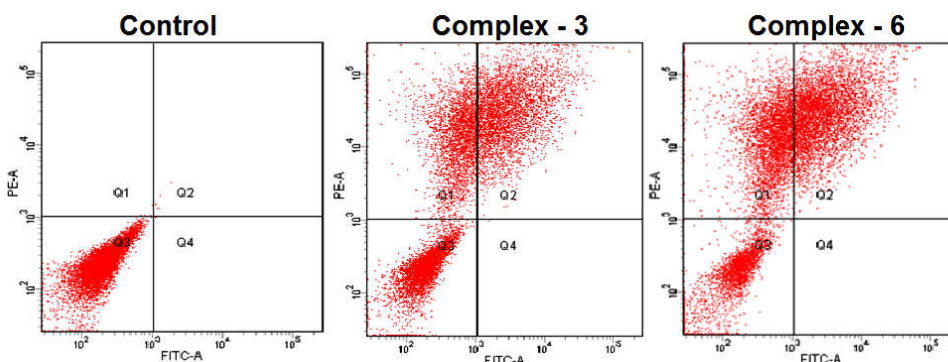


508  
509 **Figure 5.** Morphological assessment of complexes **3** and **6** ( $IC_{50}$  concentration) and  
510 MDA-MB-231 cells for 24 h. The scale bar 20  $\mu$ m.

511

### 512 Evaluation of apoptosis - Flow cytometry

513 The potential to induce apoptosis in cancer cells by the addition of synthesized complexes  
514 can be quantitatively investigated by flow cytometry analysis by Annexin V  
515 protocol, with the help of Annexin V-FITC Apoptosis Detection Kit to perform double-  
516 staining with propidium iodide and Annexin V-FITC. Annexin V, a  $Ca^{2+}$  dependent  
517 phospholipid-binding protein with a high affinity for the membrane phospholipid  
518 phosphatidylserine (PS), is quite helpful for identifying apoptotic cells with exposed PS.  
519 Propidium iodide is a standard flow cytometric viability probe used to distinguish viable from  
520 non-viable cells (Figure 6). The MDA-MB-231 cells were treated with the complexes **3** and  
521 **6** at  $IC_{50}$  concentrations for 24 h. The cell death induced by the complexes follow a pathway  
522 from lower left quadrant to the upper right quadrant (Annexin V<sup>+</sup>/PI<sup>+</sup>) which represents cells  
523 undergoing apoptosis.<sup>30</sup>



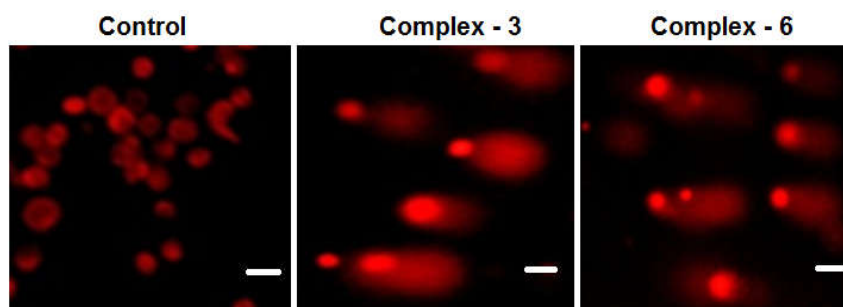
524

525 **Figure 6.** AnnexinV/propidium iodide assay of MDA-MB-231 cells treated by complexes **3**  
 526 and **6** ( $IC_{50}$  concentration) measured by flow cytometry.

527

### 528 Comet assay

529 The Comet Assay (single-cell gel electrophoresis) in an agarose gel matrix was used to  
 530 study DNA fragmentation. The comet assay was performed with treated MDA-MB-  
 531 231 cancer cells with  $IC_{50}$  concentration of complexes **3** and **6**, large and well-rounded  
 532 comets are observed while the control cells fail to show a comet like appearance  
 533 (Figure 7). The comet score for complexes **3** and **6** shows significant number of  
 534 nucleoids with larger comet tails, indicative of higher levels of DNA single-strand  
 535 breaks.<sup>31</sup>



536

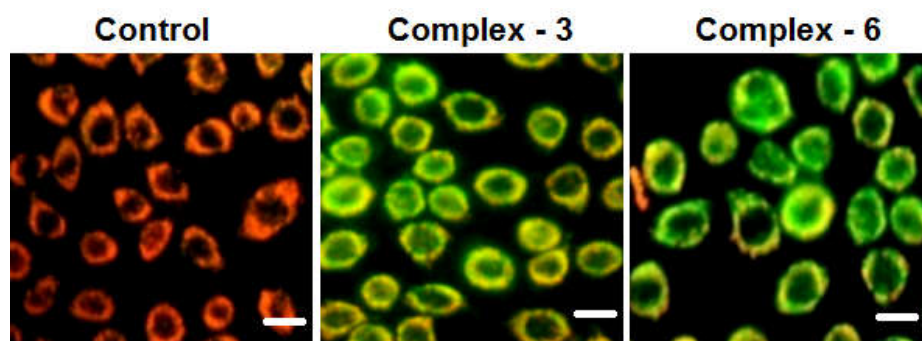
537 **Figure 7.** Comet assay of staining of EB control (untreated) treated with complexes **3** and **6**  
 538 ( $IC_{50}$  concentration) for 24 h. The scale bar 40  $\mu$ m.

539

### 540 Mitochondrial membrane potential detection

541 Mitochondria act as a point of integration for apoptotic signals originating from both  
 542 extrinsic and intrinsic apoptotic pathways. Mitochondria play important roles in  
 543 apoptosis through the release of proapoptotic factors such as cytochrome *c* and other  
 544 apoptosis-inducing factors. The changes in mitochondrial membrane potential were  
 545 detected using the fluorescent probe JC-1. It exhibits potential-dependent

546 accumulation in mitochondria, indicated by a fluorescence emission shift from red  
547 (~590 nm) to green (~525 nm). As shown in Fig, in the control, JC-1 emits red  
548 fluorescence. When the MDA-MB-231 cells were treated with the complexes, JC-1  
549 displays a green fluorescence. The changes from red to green fluorescence indicate the  
550 decrease of mitochondrial membrane potential (Figure 8). These results suggest that  
551 complexes **3** and **6** can induce the decrease of mitochondrial membrane potential.<sup>32</sup>



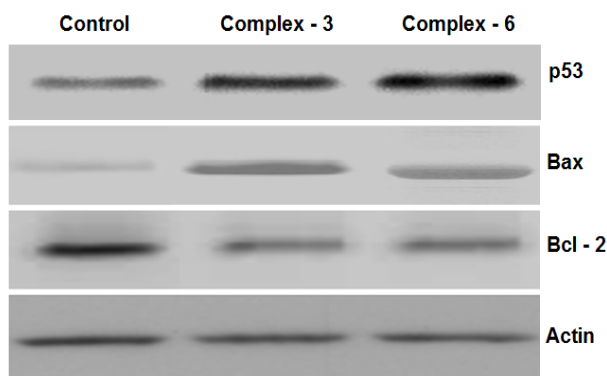
552  
553 **Figure 8.** MDA-MB-231 cells were treated with complexes **3** and **6** (IC<sub>50</sub> concentration) for  
554 24 h. The scale bar 20 μm

555  
556

### 557 **Western blot analysis**

558 To reveal the underlying mechanism behind the antiproliferative activity of Ru(II)  
559 benzhydrazone complexes, Western blot technique has been employed. It is  
560 established that apoptic proteins like p53, Bax and anti-apoptotic protein Bcl-2 play a  
561 pivotal role during the induction of apoptosis. The expression level of p53, Bax and  
562 Bcl-2 proteins were analyzed in the **3** and **6** treated MDA-MB-231 cells and control  
563 cells. It is observed that the expression level of the Bcl-2 protein decreases suggesting  
564 that apoptosis by **3** and **6** could be mediated through the downregulation of the  
565 antiapoptotic protein Bcl-2. The p53 and Bax proteins level in MDA-MB-231 cancer  
566 cell lines is remarkably increased upon treatment with the complexes revealing that the  
567 complexes induce apoptosis (Figure 9). Hence, the upregulation of proapoptotic  
568 protein Bax, p53 and the downregulation of antiapoptotic protein Bcl-2 caused by  
569 complexes **3** and **6** could possibly activate mitochondria-mediated apoptosis.<sup>33</sup>

570



571

572

573 **Figure 9.** Western blot of p53, Bax and Bcl-2 proteins in MDA-MB-231 cells. Lane-1  
574 control, lanes-2 and 3 treated with the complexes **3** and **6** ( $IC_{50}$  concentration).  $\beta$ -Actin  
575 as a loading control.

576

## 577 Conclusions

578 An easy route of synthesis of six new ruthenium(II) arene indole-3-carboxaldehyde  
579 benzhydrazone has been described for the first time. The characterization of the complexes  
580 (**1-6**) was accomplished by analytical and spectral methods (IR, UV-vis,  $^1H$  and  $^{13}C$  NMR  
581 and ESI-MS). X-ray diffraction study reveals that the benzhydrazone ligand coordinated to  
582 ruthenium *via* azomethine nitrogen and imidolate oxygen and adopts the familiar pseudo-  
583 octahedral “piano-stool” geometry. Interestingly, the cytotoxic activities of complex **6**  
584 against the tested cancer cell lines were significantly superior to that of the well-  
585 known anticancer drug cisplatin and the observed high cytotoxicity is correlated with  
586 nature of the substituent of the ligand and arene moiety. Furthermore, fluorescence  
587 staining techniques and flow cytometry using the annexin-V assay revealed that  
588 complexes **3** and **6** induce apoptosis in MDA-MB-231 cancer cells. Further alkaline  
589 comet assay confirms the single-strand break of DNA. The results of mitochondrial  
590 membrane potential and Western blot analysis demonstrated that the complexes with potent  
591 antiproliferative activity are able to induce mitochondria - mediated apoptosis in human  
592 cancer cells. On the basis of the results, we suggest that ruthenium arene benzhydrazone  
593 complexes may be the best candidates for further evaluation as chemopreventive and  
594 chemotherapeutic agents for human cancers.

595

596

597

## 598 Acknowledgements

599 One of the authors (MKMS) thank the University Grants Commission (UGC), New Delhi for  
600 financial assistance through the UGC-BSR fellowship (Ref. No. F.7-22/2007(BSR)). We  
601 express sincere thanks to DST-FIST, India for the use of Bruker 400 MHz spectrometer at the  
602 School of Chemistry, Bharathidasan University, Tiruchirappalli-24.

603

## 604 Supporting Information

605 CCDC deposition No. 1499166 (**3**) and 1498893 (**6**) contain the supplementary  
606 crystallographic data for this paper. In addition, selected crystal data and structure refinement  
607 data and Figures contain the  $^1\text{H}$  and  $^{13}\text{C}$  NMR, ESI-MS, UV-vis spectrum and Intermolecular  
608 interaction diagrams of complexes **3** and **6** are provided.

609

## 610 References

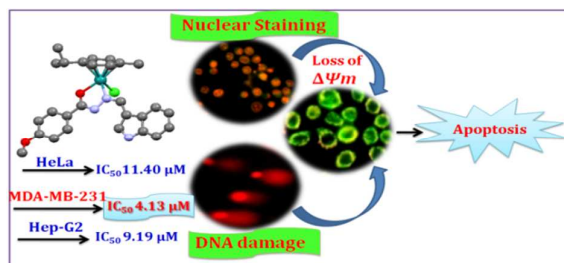
- 611 1. L. Kelland, *Nat Rev Cancer*, 2007, **7**, 573-584.
- 612 2. (a) L. X. Cubeddu, I. S. Hoffmann, N. T. Fuenmayor and A. L. Finn, *N. Engl. J. Med.*  
613 1990, **322**, 810-816; (b) M. A. Jakupec, M. Galanski, V. B. Arion, C. G. Hartinger and B. K.  
614 Keppler, *Dalton Trans.* 2008, 183-194.
- 615 3. P. J. Dyson and G. Sava, *Dalton Trans.* 2006, 1929-1933.
- 616 4. G. Sava, A. Bergamo, S. Zorzet, B. Gava, C. Casarsa, M. Cocchietto, A. Furlani, V.  
617 Scarcia, B. Serli, E. Iengo, E. Alessio and G. Mestroni, *Eur. J. Cancer* 2002, **38**, 427-435.
- 618 5. R. Trondl, P. Heffeter, C. R. Kowol, M. A. Jakupec, W. Berger and B. K. Keppler, *Chem.*  
619 *Sci.* 2014, **5**, 2925-2932.
- 620 6. (a) A. L. Noffke, A. Habtemariam, A. M. Pizarro and P. J. Sadler, *Chem. Comm.* 2012, **48**,  
621 5219-5246; (b) R. E. Aird, J. Cummings, A. A. Ritchie, M. Muir, R. E. Morris, H. Chen, P. J.  
622 Sadler and D. I. Jodrell, *Br J Cancer*, 2002, **86**, 1652-1657; (c) G. Suss-Fink, *Dalton Trans.*  
623 2010, **39**, 1673-1688; (d) A. A. Nazarov, C. G. Hartinger and P. J. Dyson, *J. Organomet.*  
624 *Chem.* 2014, **751**, 251-260; (e) R. Pettinari, F. Marchetti, C. Pettinari, A. Petrini, R.  
625 Scopelliti, C. M. Clavel and P. J. Dyson, *Inorg. Chem.* 2014, **53**, 13105-13111; (f) L. E. H.  
626 Paul, B. Therrien and J. Furrer, *Inorg. Chem.* 2012, **51**, 1057-1067; (g) M. Melchart, A.  
627 Habtemariam, O. Novakova, S. A. Moggach, F. P. A. Fabbiani, S. Parsons, V. Brabec and P.  
628 J. Sadler, *Inorg. Chem.* 2007, **46**, 8950-8962; (h) R. K. Gupta, G. Sharma, R. Pandey, A.  
629 Kumar, B. Koch, P.-Z. Li, Q. Xu and D. S. Pandey, *Inorg. Chem.* 2013, **52**, 13984-13996.

- 630 7. H. Chen, J. A. Parkinson, R. E. Morris and P. J. Sadler, *J. Am. Chem. Soc.* 2003, **125**, 173-  
631 186.
- 632 8. A. Kurzwernhart, W. Kandioller, S. Bächler, C. Bartel, S. Martic, M. Buczkowska, G.  
633 Mühlgassner, M. A. Jakupec, H.-B. Kraatz, P. J. Bednarski, V. B. Arion, D. Marko, B. K.  
634 Keppler and C. G. Hartinger, *J. Med. Chem.* 2012, **55**, 10512-10522.
- 635 9. W. Su, Q. Qian, P. Li, X. Lei, Q. Xiao, S. Huang, C. Huang and J. Cui *Inorg. Chem.* 2013,  
636 **52**, 12440-12449.
- 637 10. R. Pettinari, C. Pettinari, F. Marchetti, B. W. Skelton, A. H. White, L. Bonfili, M.  
638 Cuccioloni, M. Mozzicafreddo, V. Cecarini, M. Angeletti, M. Nabissi and A. M. Eleuteri, *J.*  
639 *Med. Chem.* 2014, **57**, 4532-4542.
- 640 11. C. M. Clavel, E. Păunescu, P. Nowak-Sliwinska, A. W. Griffioen, R. Scopelliti and P. J.  
641 Dyson, *J. Med. Chem.* 2015, **58**, 3356-3365.
- 642 12. Q. Wu, K. Zheng, S. Liao, Y. Ding, Y. Li and W. Mei, *Organometallics*, 2016, **35**, 317-  
643 326.
- 644 13. (a) T. Nasr, S. Bondock and M. Youns, *Eur J Med Chem.* 2014, **76**, 539-548; (b) T.  
645 Giraldi, P. M. Goddard, C. Nisi and F. Sigon, *J. Pharm. Sci.* 1980, **69**, 97-98.
- 646 14. (a) M. Varache-Lembège, S. Moreau, S. Larrouture, D. Montaudon, J. Robert and A.  
647 Nuhrich, *Eur J Med Chem.* 2008, **43**, 1336-1343; (b) H. A. Abdel-Aziz, T. Aboul-Fadl, A.-R.  
648 M. Al-Obaid, M. Ghazzali, A. Al-Dhfyan and A. Contini, *Arch. Pharmacol Res.* 2012, **35**,  
649 1543-1552.
- 650 15. (a) M. Alagesan, P. Sathyadevi, P. Krishnamoorthy, N. S. P. Bhuvanesh and N.  
651 Dharmaraj, *Dalton Trans.* 2014, **43**, 15829-15840; (b) E. Singleton and H. E. Swanepoel,  
652 *Inorg. Chim. Acta.* 1982, **57**, 217-221.
- 653 16. (a) J. Fernandez-de-Cossio, *Analytical Chemistry*, 2010, **82**, 1759-1765; (b) IsoPro,  
654 version 3.1; Cornell University. A computer program written by Michael W. Senko that  
655 implements Yergey's polynomial method running under Microsoft Windows.
- 656 17. (a) M. A. Bennett and A. K. Smith, *J. Chem. Soc., Dalton Trans.* 1974, 233-241; (b) M.  
657 A. Bennett, T. N. Huang, T. W. Matheson, A. K. Smith, S. Ittel and W. Nickerson, in ., *Inorg.*  
658 *Synth.*, 1982, 74-78.
- 659 18. A. R. B. Rao and S. Pal, *J. Organomet. Chem.* 2011, **696**, 2660-2664.
- 660 19. G. Sheldrick, *Acta Crystallographica Section A*, 2008, **64**, 112-122.
- 661 20. L. Farrugia, *J. Appl. Crystallogr.* 1997, **30**, 565.
- 662 21. (a) R. J. Butcher, J. Jasinski, G. M. Mockler and E. Sinn, *J. Chem. Soc. Dalton Trans.*  
663 1976, 1099-1102 ;(b) R. N. Prabhu and R. Ramesh, *RSC Adv.* 2012, **2**, 4515-4524.



- 664 22. K. N. Kumar, G. Venkatachalam, R. Ramesh and Y. Liu, *Polyhedron*, 2008, **27**, 157-166.
- 665 23. (a) M. U. Raja and R. Ramesh, *J. Organomet. Chem.* 2012, **699**, 5-11; (b) M. Kalidasan,  
666 R. Nagarajaprakash, S. Forbes, Y. Mozharivskyj and K. M. Rao, *Z. Anorg. Allg. Chem.* 2015,  
667 **641**, 715-723.
- 668 24. F. Marchetti, C. Pettinari, R. Pettinari, A. Cerquetella, C. Di Nicola, A. Macchioni, D.  
669 Zuccaccia, M. Monari and F. Piccinelli, *Inorg. Chem.* 2008, **47**, 11593-11603; (b) (b) D.  
670 Pandiarajan and R. Ramesh, *J. Organomet. Chem.* 2013, **723**, 26-35.
- 671 25. (a) J. Valladolid, C. Hortiguera, N. Busto, G. Espino, A. M. Rodriguez, J. M. Leal, F. A.  
672 Jalon, B. R. Manzano, A. Carbayo and B. Garcia, *Dalton Trans.* 2014, **43**, 2629-2645; (b) F.  
673 Aman, M. Hanif, W. A. Siddiqui, A. Ashraf, L. K. Filak, J. Reynisson, T. Söhnel, S. M. F.  
674 Jamieson and C. G. Hartinger, *Organometallics*, 2014, **33**, 5546-5553; (c) X. Lei, W. Su, P.  
675 Li, Q. Xiao, S. Huang, Q. Qian, C. Huang, D. Qin and H. Lan, *Polyhedron*, 2014, **81**, 614-  
676 618.
- 677 26. (a) A. Habtemariam, M. Melchart, R. Fernández, S. Parsons, I. D. H. Oswald, A. Parkin,  
678 F. P. A. Fabbiani, J. E. Davidson, A. Dawson, R. E. Aird, D. I. Jodrell and P. J. Sadler, *J.*  
679 *Med. Chem.* 2006, **49**, 6858-6868; (b) R. E. Morris, R. E. Aird, P. del Socorro Murdoch, H.  
680 Chen, J. Cummings, N. D. Hughes, S. Parsons, A. Parkin, G. Boyd, D. I. Jodrell and P. J.  
681 Sadler, *J. Med. Chem.* 2001, **44**, 3616-3621.
- 682 27. (a) L. He, S.-Y. Liao, C.-P. Tan, R.-R. Ye, Y.-W. Xu, M. Zhao, L.-N. Ji and Z.-W. Mao,  
683 *Chem. Eur. J.* 2013, **19**, 12152-12160; (b) Q. Wu, C. Fan, T. Chen, C. Liu, W. Mei, S. Chen,  
684 B. Wang, Y. Chen and W. Zheng, *Eur. J. Med. Chem.* 2013, **63**, 57-63; (c) Q. Wu, K. Zheng,  
685 S. Liao, Y. Ding, Y. Li and W. Mei, *Organometallics*, 2016, **35**, 317-326.
- 686 28. R. K. Gupta, R. Pandey, G. Sharma, R. Prasad, B. Koch, S. Srikrishna, P.-Z. Li, Q. Xu  
687 and D. S. Pandey, *Inorg. Chem.* 2013, **52**, 3687-3698.
- 688 29. (a) Z.-F. Chen, Q.-P. Qin, J.-L. Qin, Y.-C. Liu, K.-B. Huang, Y.-L. Li, T. Meng, G.-H.  
689 Zhang, Y. Peng, X.-J. Luo and H. Liang, *J. Med. Chem.* 2015, **58**, 2159-2179; (b) J. P.  
690 Johnpeter, G. Gupta, J. M. Kumar, G. Srinivas, N. Nagesh and B. Therrien, *Inorg. Chem.*  
691 2013, **52**, 13663-13673.
- 692 30. B. Banik, K. Somyajit, G. Nagaraju and A. R. Chakravarty, *Dalton Trans.* 2014, **43**,  
693 13358-13369.
- 694 31. R. M. Lord, A. J. Hebden, C. M. Pask, I. R. Henderson, S. J. Allison, S. L. Shepherd, R.  
695 M. Phillips and P. C. McGowan, *J. Med. Chem.* 2015, **58**, 4940-4953.

- 696 32. (a) C. Qian, J.-Q. Wang, C.-L. Song, L.-L. Wang, L.-N. Ji and H. Chao, *Metallomics*,  
697 2013, **5**, 844-854; (b) R. Cao, J. Jia, X. Ma, M. Zhou and H. Fei, *J. Med. Chem.* 2013, **56**,  
698 3636-3644.
- 699 33. (a) A. J. Levine, J. Momand and C. A. Finlay, *Nature*, 1991, **351**, 453-456; (b) (b) J. C.  
700 Reed, *J. Cell. Biol.* 1994, **124**, 1-6; (c) T. Chen, Y. Liu, W.-J. Zheng, J. Liu and Y.-S. Wong,  
701 *Inorg. Chem.* 2010, **49**, 6366-6368.



A series of ruthenium(II) arene complexes have been synthesized and evaluated for their *in vitro* anticancer activities. The complex exhibits promising anticancer activity in human cancer cells.